Characteristics and Identification of Partial Discharge for Insulation Structures in High Voltage IGBT Modules Under Positive Square Wave Voltage

Xiangchen Liu, Xuebao Li, Chao Li, Jinjin Cheng, Zhaocheng Liu, Zhibin Zhao, Xiang Cui, *Senior Member, IEEE*, Xiaoguang Wei, and Xinling Tang

***Abstract*—The insulation of insulated gate bipolar transistor (IGBT) modules is one of the key constraint factors in module development. It is significant to realize the accurate measurement of partial discharge (PD) and its identification of the insulation weaknesses under positive square wave voltage. In this article, a PD experimental platform under this voltage is established. Three main possible insulation weaknesses of high voltage IGBT modules are selected as experimental samples, including chip, silicone gel, and the interface between direct bonded copper and silicone gel. Then, PD current waveforms of them are measured. To solve the interference caused by high *du/dt* at the rising/falling edge of voltage, a distortionless extraction method of PD pulses independent of any auxiliary detection equipment is proposed. Based on this method, the PD phase distributions of three samples are obtained and there are distinct differences among them. Thus, the PD types in high voltage modules can be identified effectively. In addition, qualitative explanations of the differences in the typical PD characteristics are presented. The proposed PD identification method is experimentally verified and can guide the insulation design and fabrication of high voltage IGBT modules.**

***Index Terms*—Positive square wave voltage, high voltage IGBT, partial discharge (PD) pulses extraction, PD identification.**

I. Introduction

HIGH voltage insulated gate bipolar transistor (IGBT) has the advantages of fast switching speed, low saturation voltage, and high current density. IGBT is the core component of large capacity converter equipment and has been widely used in the fields of new energy grid-connection and high voltage direct current transmission [1], [2].

With the development of high voltage IGBT module, the rated voltage of the IGBT module is greatly increased from 6.5 kV for Si IGBT modules to 27 kV for SiC IGBT modules [3]. At this high voltage, the insulation reliability of insulating materials used in the module's internal packaging is one of the crucial factors for the safe and stable operation of the module. While the dielectric strength of protective gas used in press-pack IGBT modules is much lower than that of silicone gel used in wire-bond and StakPak IGBT modules. Thus, the wire-bond and StakPak modules may have better application prospects for the higher voltage demand in the future [4].

Structures of the wire-bond and StakPak IGBT are shown in Fig. 1, in which the high voltage electrode is red. There are several main voltage bearing structures, including the silicone gel, direct bonded copper (DBC), and chip as shown in Fig. 1. Furthermore, the IGBT module works in the states of repeating turn-ON and turn-OFF. Thus, the module insulation bears a positive repetitive square wave voltage [5]. Under this voltage, the insulation of the module package is prone to partial discharge (PD), which may lead to insulation deterioration and even breakdown eventually [6], [7].

As shown in Fig. 2(a), the bubble in the silicone gel of a StakPak IGBT module is generated by violent PDs during the experiment, located between the wire bond and the DBC. What's more, the triple point of DBC has also been reported to be the possible PD occurrence position in IGBT modules by researchers through simulations and experiments [8], [9], [10], [11]. Besides, the damage position left after the breakdown of the chip can also be seen in Fig. 2(b).

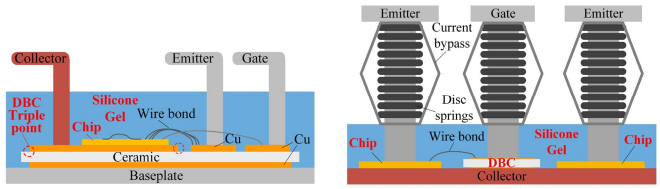

Fig. 1. Structures of modules. (a) Wire-bond IGBT. (b) StakPak IGBT.

Manuscript received 6 July 2022; revised 19 September 2022; accepted 21 December 2022. Date of publication 27 December 2022; date of current version 14 February 2023. This work was supported by the Science and Technology Project of State Grid under Grant 5500-202158435A-0-0-00. Recommended for publication by Associate Editor M. Nawaz. *(Corresponding author: Xuebao Li.)*

Xiangchen Liu, Xuebao Li, Chao Li, Jinjin Cheng, Zhaocheng Liu, Zhibin Zhao, and Xiang Cui are with the State Key Laboratory of Alternate Electrical Power System with Renewable Energy Sources, North China Electric Power University, Beijing 102206, China (e-mail: 120202201087@ncepu.edu.cn; lxb08357x@ncepu.edu.cn; lichao_ncepu@126.com; cjj07018@163.com; zc.liu@ncepu.edu.cn; zhibinzhao@126.com; x.cui@ncepu.edu.cn).

Xiaoguang Wei and Xinling Tang are with the State Key Laboratory of Advanced Power Transmission Technology, Smart Grid Institute Co., Ltd., Beijing 102209, China (e-mail: weixiaoguang@geiri.sgcc.com.cn; 18817555671@126.com).

Color versions of one or more figures in this article are available at https://doi.org/10.1109/TPEL.2022.3232327.

Digital Object Identifier 10.1109/TPEL.2022.3232327

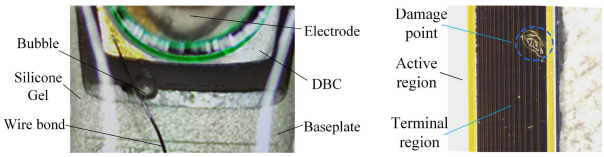

Fig. 2. Common module discharge positions. (a) Bubbles in the silicone gel. (b) Damage point of chip.

At the early stage, many excellent investigations have been carried out for the PD characteristics of silicone gel and DBC-silicone gel interface of IGBT modules. Do et al. [12], [13] conducted PD experiments on silicone gel by using a point-plane gap. The influence of temperature on the PD inception voltage (PDIV) under ac voltage and the influence of different voltage waveforms on silicone gel electrical tree were reported. Yabuuchi et al. [14] investigated the development of electrical trees caused by PD under ac voltage in silicone gel with needle-plate electrode structure. Through simulations and experiments, ABB researchers found that the most critical causes for insulation failure are protrusions and field enhancements due to imperfect etch shapes of DBC [7]. PD experiments were carried out on the DBC-silicone gel interface, and the effect of ac voltage frequency on the discharge was studied by Masahiro Sato [10]. In fact, the abovementioned investigation focused more on the PD characteristics under ac or dc voltage. However, the PD characteristics under square wave voltage are different from those under ac and dc voltage, which have been proved and realized by many researchers [15], [16], [17].

In recent years, many researchers have conducted the PD characteristics of the insulation structures of IGBT modules under square wave voltage. Mancinelli et al. [17] studied the influences of frequency, rise time, and polarity on silicone gel electrical treeing under square voltage. Fu et al. [18] conducted experimental investigations on the discharge characteristics of the interface between the PEEK and N_2 under positive square wave voltage. In 2019, the development characteristics of electrical trees in silicone gel under repetitive square voltage were reported by Nakamura et al. [19]. Wang et al. [15], [20] investigated the difference of power module PDs under dc and pulsewidth modulation waveforms. Lin et al. [21] investigated the influences of temperature and operation duration on the maximum electric field stress in wire-bonding modules under square wave voltage. Besides, the influence of the repetitive frequency and rise time of positive square wave voltage on the PD characteristics for the DBC-silicone gel was studied firstly by Mancinelli et al. [17], which is of great reference value. Therefore, the discharge characteristics of the insulation structures in the IGBT modules should be carried out under positive square wave voltage for guiding the insulation design for the IGBT modules. Besides, through comparisons of the discharge differences for the different insulation structures, the PD position in the IGBT modules may be identified [22], [23]. As for the three insulation structures in the high voltage IGBT module mentioned above, i.e. the silicone gel, DBC-silicone gel interface, and chip, the PD characteristics under positive square wave voltage have not been systematically investigated before, especially for the PD characteristics of chips.

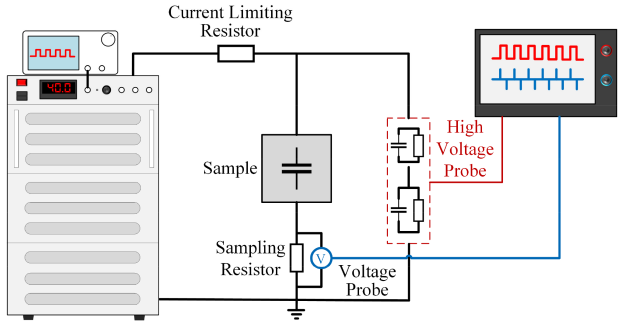

Fig. 3. PD Experiment setup circuit.

In fact, for the accurate measurement of the PD current pulses under positive square wave voltage, the main obstacle is how to remove the interference caused by the high *du/dt* during the rise and fall of the square wave voltage. For the measurement of PD under short rise time and repetitive voltage impulses, the coupling capacitor with filter, high frequency current transformer (HFCT) with filter, and ultra high frequency (UHF) antenna were given by IEC/TS 61934 [24]. For the UHF antenna, the measured results are not quantitative and may be affected by the position of the antenna [15]. Thus, considering the possible practical application in the future, simple measurement and analysis methods based on HFCT for the PD characteristics of the insulation structures in the high voltage IGBT module under positive square wave voltage are required.

In this article, a PD experiment platform is established for measurement of the PD characteristics under positive square wave voltage of silicone gel, DBC-silicone gel interface, and chip, which are the typical insulation structures in the high voltage IGBT module. The discharge current waveforms for three structures are measured, respectively. Then, a method that can accurately separate PD current pulses from displacement current is proposed. After that, the PD characteristics under positive square wave voltage of the above typical structures are investigated, which can be used as the identification and classification features for discharges of the three typical structures. Then, the validity of the proposed identification method is verified by the experiment. Finally, the qualitative mechanism explanations for discharge under the positive square wave of the three typical structures are presented.

II. Experiment Setup and Experiment Procedure

A. Experiment Platform Setup

The experimental platform shown in Fig. 3 is developed to measure PD current pulses of the typical insulation structures in the high voltage IGBT module under square wave voltage. In the experiments, the positive square wave voltage source is applied to the above-mentioned sample through the current limiting resistor. The experimental sample is grounded through the sampling resistor with a value of 500 Ω. The square wave voltage source is composed of the AFG3022C signal generator

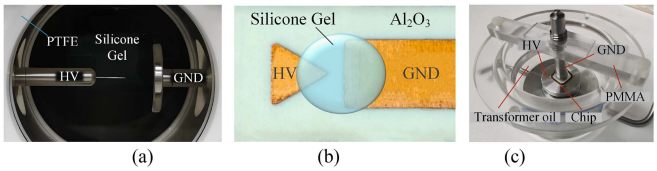

Fig. 4. Schematic diagram of three experimental samples. (a) Silicone gel. (b) DBC-silicone gel interface. (c) Chip.

of Tektronix and the AMP 40B20 voltage amplifier of Matsusada. The voltage amplifier can amplify the signal generator signal 4000 times, and the protection resistor is a non-PD resistor with a value of 10 kΩ. The maximum voltage is up to 40 kV and the minimum rise time is 20 μs for the positive square wave voltage.

Besides, the applied voltage on the experimental sample is measured by a high voltage probe typed as North Star PVM-4. The measurement range of the high voltage probe is from -100 to 100 kV with a 1000:1 attenuation ratio and measurement accuracy of ±4 V. The PD pulse is only measured through the sampling resistor by a broadband voltage probe typed as Teledyne LeCroy PP-018. In the experiments, the applied positive square wave voltage and the PD current signals are measured simultaneously by the oscilloscope with a sampling rate of 250 MS/s.

B. Experimental Samples

According to the analysis of the typical voltage-bearing structures of high voltage modules in Chapter I, silicone gel, DBC-silicone gel interface, and chip are selected to be the experimental samples. In the experiments, samples as shown in Fig. 4 are designed to approach the defects and electrode structure in high voltage IGBT module as soon as possible:

In case 1, the silicone gel under needle-plate electrodes is shown in Fig. 4(a). The silicone gel used in the experiment is a commercial two-component additive silicone gel, which is prepared in the lab by mixing components A and B. The mixed sample should be cleaned, dried, and degassed using the steps described in [25], which can insure as few bubbles as possible in the silicone gel. The needle-plate electrode, which was usually employed to investigate the insulation characteristics of silicone gel [12], [13], [14], [17], is used to investigate the internal discharges in the silicone gel of module encapsulation. The electrode spacing is set to 10 mm, which is better to complete data acquisition without breakdown. The diameter of the needle tip and the plate are 30 μm and 30 mm, respectively. The material of the needle plate electrode is stainless steel. The mold is made of PTFE and PEEK insulation materials to eliminate possible discharge caused by suspension potential.

In case 2, the tip plate electrode structure with double-sided copper cladding shown in Fig. 4(b) is adopted for the following two reasons. First, to simulate the tiny copper protrusion, which is hard to avoid during DBC's metallization due to technological limitations [7]. Second, to create the high electric field locally to investigate the surface discharges on DBC's ceramic, which is different from the internal discharge in the silicone gel. In fact, the electrode structure covered by silicone gel was usually adopted to investigate the insulation characteristics of DBC-silicone gel interface [6], [10]. In the experiments, the electrode material is copper, and the material of the ceramic substrate is Al_2O_3. The electrode spacing is set to 2 mm, referring to the width between DBC's metallization in high voltage wire-bond modules. The silicone gel used is degassed with the same process as mentioned in case 1.

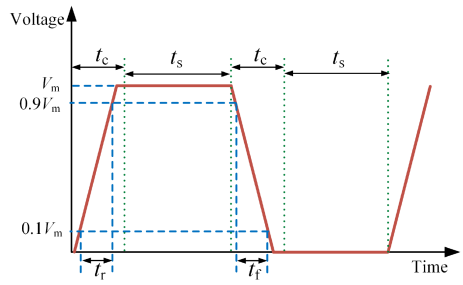

Fig. 5. Square wave voltage waveform [18].

In case 3, a 3300 V high voltage chip is packed by the column-plate electrode as shown in Fig. 4(c) to simulate the package form of the chip in StakPak modules. The diameter of the cylindrical electrode and the bottom plane electrode is 6 and 30 mm, respectively. The electrodes are fixed in a transparent acrylic cavity. Besides, to eliminate the possible discharge that occurred at the terminal surface of the chip and air, and the possible defect in silicone gel, transformer oil is used for encapsulation in the experiment. A no-load test is carried out for the transformer oil before the experiment to confirm that no PD occurs under the breakdown voltage of the chip.

C. Voltage Waveform and Experiment Procedure

The positive polarity square wave voltage applied in the experiment is shown in Fig. 5. The high-level amplitude V_m is adjustable. The low level is set to 40 V to prevent the instantaneous voltage from falling below zero due to voltage ripple. The voltage duty ratio is 50%, and the repetitive frequency is 50 Hz. The rise time (t_r) and fall time (t_f) are both 20 μs. Due to the transient overshoot of square wave voltage, the voltage variation period (t_c) is 0.05 ms, and the voltage steady-state period (t_s) is 9.95 ms.

Before the experiment, a no-load test is carried out first, and no PD signal is detected when the voltage is applied to 30 kV. According to the standard of PD measurement [26], the speed of voltage increase is set as 80 V/s before 70% of the estimated PDIV. Then, the voltage is increased at the speed of 8 V/s until five PD pulses appear on average in ten cycles. The voltage at this point is the repeated PD initiation voltage (RPDIV).

III. Experiment Results and Pulse Extraction

A. Basic Characteristics of the Experimental Results

The voltage and current waveforms within five cycles of the three samples when PD occurs are shown in Fig. 6. The blue line is the voltage signal, and the red line is the current signal.

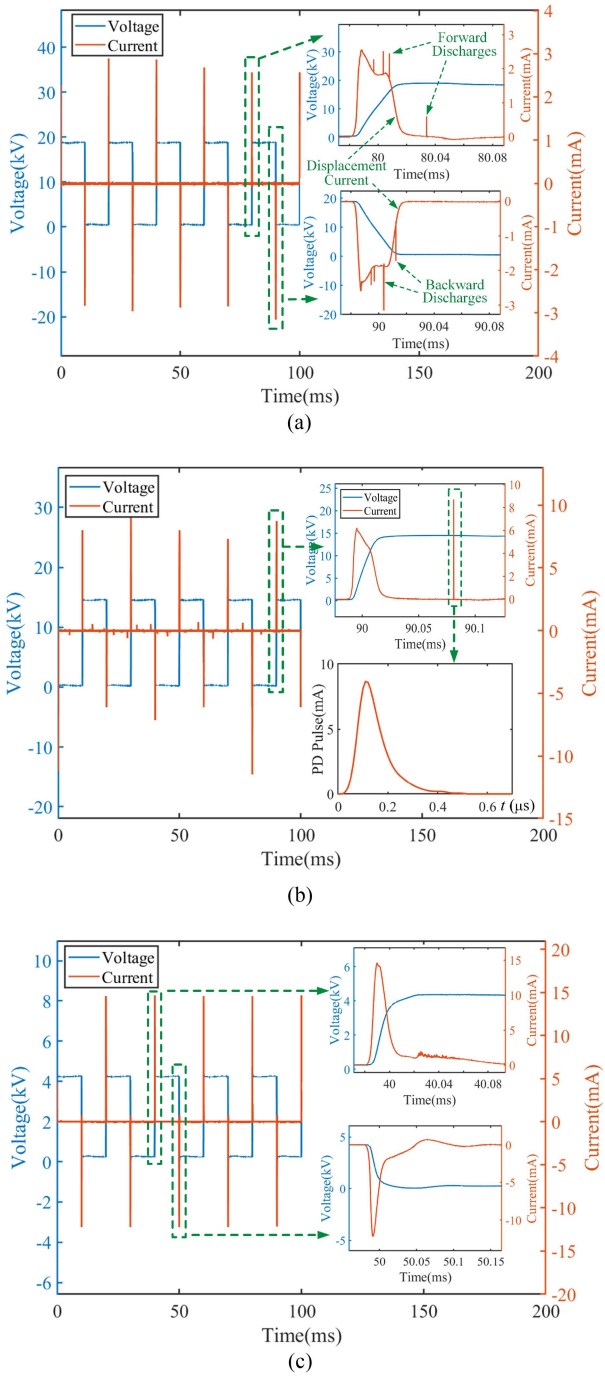

Fig. 6. Voltage and current signals of samples. (a) Silicone gel. (b) DBC-Silicone gel interface. (c) Chip.

Since samples can be approximated as a capacitance, the displacement current can be measured in the circuit under the action of the high *du/dt* at the rising and falling of the square wave voltage. Besides, the forward discharges current pulses, whose waveform fits the double exponential pulses, can be generated at the rising process and high level of the applied voltage. While backward discharges current pulses with negative polarity are generated at the falling process and low level of the applied voltage both for the discharges in silicone gel and DBC-silicone gel interface. For the discharge pulses in silicone gel, most forward and backward current pulses concentrate on the displacement current pulses, and multiple discharge pulses can be generated in one cycle. But for the discharge pulses from the DBC-silicone gel interface, some discharge current pulses with smaller amplitude are distributed in voltage steady-state. Furthermore, for the discharges in the chip, only multiple positive polarity current pulses are generated at the high level of the applied voltage and no backward discharge occurs. The obtained differences can provide the possibility to identify the discharge type. However, PD current pulses may be superimposed on the displacement current, which will impede the further investigation of PD pulse characteristics. So, the discharge current pulses should be extracted from the displacement current first.

B. PD Pulse Extraction

Some of the existing PD detection methods used by researchers are given in Table I.

For the methods based on HFCT, the auxiliary equipment seems to be needed to identify or extract the PD current pulses from the displacement current interface [11], [27], resulting in inconvenience for the actual measurement of the PD current pulses.

Besides, an appropriate filter may be another good choice to obtain accurate PD current pulses. So, the characteristics of the displacement current pulses and PD current pulses should be analyzed. Since the PD current pulse is not available, it is necessary to analyze the displacement current and discharge pulse theoretically before the extraction.

In fact, the typical square wave voltage $u(t)$ can be expressed as

$$u(t) = k_1 t - k_1(t-t_r)\varepsilon(t-t_r) - k_2(t-T/2)\varepsilon(t-T/2) + k_2(t-T/2-t_f)\varepsilon(t-T/2-t_f) \quad (1)$$

$$k_1 = U_m/t_r \quad (2)$$

$$k_2 = U_m/t_f \quad (3)$$

where U_m is square wave high level amplitude, t_r and t_f are the rise and falling time of the square wave voltage, respectively, T is the period of the repeating square wave, and $\varepsilon(t)$ is the Heaviside step function.

Then, the displacement current $i_D(t)$ can be expressed as

$$i_D(t) = C \cdot du/dt \quad (4)$$

where C is the capacitance of the experimental sample.

Besides, the double exponential pulse $i_{p0}(t)$ is used to simulate the PD pulse as shown in Fig. 7(b), $i_{\mathrm{p0}}(t)$ can be expressed as

$$i_{p_0}(t) = k_3(\exp(-\alpha t) - \exp(-\beta t)) \quad (5)$$

where k_3, α, and β are the fitting parameters for the double exponential pulse.

Fig. 7(a) shows the properly smoothed typical square wave voltage in the rising process and the corresponding displacement current calculated by (4). The amplitude of the voltage is set as 18 kV, and the t_r and t_f are both set as 20 μs based on the experiments. The capacitance is estimated as 10 pF. Besides, the

TABLE I
REQUIREMENTS OF VARIOUS PD DETECTION METHODS EXISTING

Methods	Measured amount	Auxiliary equipment	Measurement environment	Signal processing	Limitation
HFCT	PD current, optical signal [11]	Optical sensor (PMT)	Dark environment	-	Constrained by environment
	PD current, optical signal [28]	Optical sensor (SiPM)	Dark environment	-	
	PD current [29]	Capacitance	-	-	Constrained by equipment
	PD current [27]	Power supply	-	-	
	PD current [30]	-	-	Wavelet Packet Transform	Signal distortion

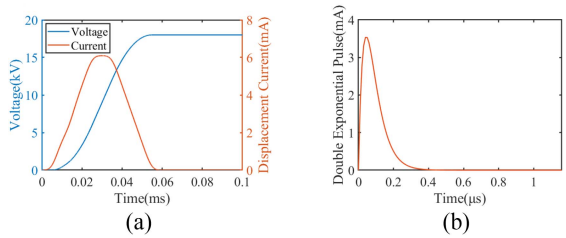

Fig. 7. Typical signal waveforms. (a) Square wave and displacement current. (b) PD pulse expressed by double exponential pulse.

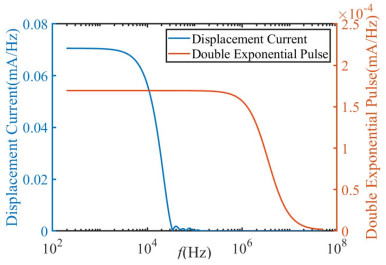

Fig. 8. Spectrum of two simulation signals.

typical waveform of PD pulse is shown in Fig. 7(b), in which k_3, α, and β are set as 43 mA, 20×10^6 s^{-1}, and 25×10^6 s^{-1}, which are precisely assigned to fit the real PD pulse.

Then, the spectral densities of the displacement current and the PD pulse shown in Fig. 7 are obtained by fast Fourier transform as shown in Fig. 8. The frequency band of the PD pulse is higher than that of the displacement current. Besides, the spectrum of displacement current and PD pulse overlaps partially.

Furthermore, to verify the above theoretical results, displacement current waveform without PD superimposed, and separate PD current pulses for samples are obtained. Then, the spectral densities of discharge current pulses and displacement current are obtained and shown in Fig. 9. The frequency bands of the discharge pulses are all higher than that of the displacement current, whose highest frequency component f_1 is about 0.3 MHz. Besides, the spectrum of displacement current and those of PD pulses from the three experimental samples overlap partially. And that will bring difficulties in the distortionless extraction of PD current through filters.

Therefore, to achieve the simple, convenient, and accurate extraction of the PD current pulses, a PD pulse extraction method is proposed. The flow chart of the method can be given in Fig. 10, which is specifically divided into the following steps.

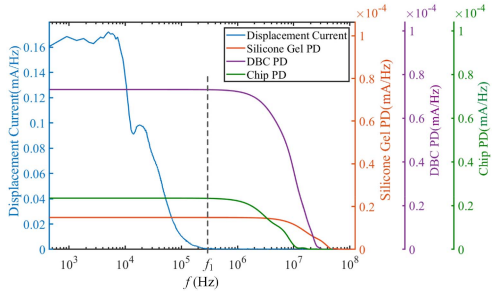

Fig. 9. Spectrum of displacement current and PD pulses.

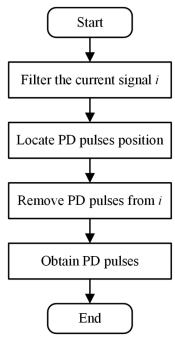

Fig. 10. Flow chart of PD pulse extraction method.

First, by filtering the original current signal $i(t)$ with a high pass filter with threshold frequency f_1, the influence of displacement current is completely removed. Then the distorted PD signal i' is obtained. In this article, the Gaussian weighted moving average filter is finally selected. Its filtering principle can be expressed as

$$i'(n) = \sum_{j=1}^{w} \{g(j) \cdot i[n + j - (w+1)/2]\} \Big/ \sum_{j=1}^{w} g(j) - i(n) \tag{6}$$

$$g(j) = \exp[-(j-(w+1)/2)^2/(2\sigma^2)]/(\sqrt{2\pi}\sigma) \tag{7}$$

where i' is the PD signal obtained by filtering, w is the width of the filtering window set as 61 in this article, σ is the standard deviation of Gaussian distribution, and g is the Gaussian function acts as the weight factor.

Second, locate the positions of the PD current pulses. Take the absolute value of i', and then find the amplitude values which are greater than the noise level. Thus, the positions of the PD

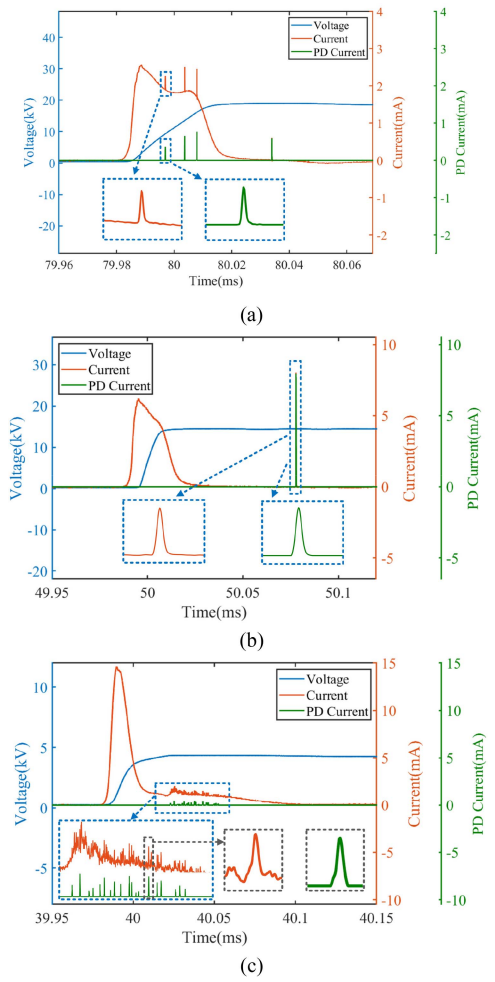

Fig. 11. Effect of pulse extraction. (a) Silicone gel, (b) DBC-Silicone gel interface. (c) Chip.

pulses (t_{pm}, $m = 1, 2, \ldots M$) in the time domain can be marked and located. M is the number of the PD current pulse amplitudes.

Third, remove the signal at the interval of [t_{pm}-t_d, t_{pm}+t_d] in the measured current waveform. The t_d is the estimated pulse width of the PD current pulses, which is set as 0.5 μs. Then, the shape-preserving piecewise cubic spline interpolation is employed to fit and fill the remaining waveform. Then, the complete displacement current waveform i_D can be obtained.

Finally, by subtracting the displacement current from the measured original current signal, the PD current pulses can be accurately acquired without any distortion.

Through the extraction method, the comparisons of the extracted PD current pulses and the measured current waveform at the rising process for the three experimental samples are given in Fig. 11. PD current pulses can be extracted from the displacement current interface without any distortions.

C. Feasibility of the PD Extraction Method

To verify the feasibility of the proposed method in extracting PD pulses under displacement current interference of square wave, displacement current waveforms $i_D(t)$ under different values of the rise time of square wave signal are calculated by using (1) and (4). Then, the double exponential pulse $i_{p0}(t)$ with known parameters is added to the displacement current waveform to simulate the waveform $i_{\mathrm{sum}}(t)$ with the PD pulse superposed on the displacement current. By using the extraction method proposed in this article, the extracted pulse from $i_{\mathrm{sum}}(t)$ is expressed as $i_{\mathrm{p}}(t)$. To calculate the correlation coefficient between $i_p(t)$ and $i_{p0}(t)$, the discretization results of them are regarded as vectors $\boldsymbol{i}_p$ and $\boldsymbol{i}_{p0}$. Then, the correlation coefficient can be expressed as the cosine of the angle θ between $\boldsymbol{i}_p$ and $\boldsymbol{i}_{p0}$, which is defined as

$$\cos\theta = \frac{\boldsymbol{ip}\cdot\boldsymbol{i}_{p_0}{}^T}{|\boldsymbol{ip}||\boldsymbol{ip}_0|} = \sum_{j=1}^{n}\boldsymbol{ip}_j\boldsymbol{ip}_{0j}\Big/\left(\sqrt{\sum_{j=1}^{n}\boldsymbol{ip}_j^2}\sqrt{\sum_{j=1}^{n}\boldsymbol{ip}_{0j}{}^2}\right). \quad (8)$$

When $\cos\theta = 1$, $i_p(t)$ and $i_{p0}(t)$ are completely positively correlated, which means $i_{p0}(t)$ is extracted from $i_{\mathrm{sum}}(t)$ without any distortion.

The correlation coefficients between $i_p(t)$ and $i_{p0}(t)$ under different rise times are given in Table II. When the rise time of the square wave is greater than 1.3 μs, the accuracy of the pulse extraction method proposed in this article can reach at least 0.9953. However, for the submicrosecond transition times, the frequency spectrum of displacement current and PD pulse overlaps too much, so it is difficult to separate the current signal by the proposed method. For PD detection under the square wave voltage of nanosecond transition times, the optical signal or UHF signal can be used to assist the detection.

So, the pulse extraction method proposed in this article is fully capable.

TABLE II
ACCURACY OF THE EXTRACTION IN DIFFERENT RISE TIME

t_r(μs)	20.0	10.0	5.0	2.0	1.5
cosθ	1.0000	1.0000	1.0000	1.0000	0.9992
t_r(μs)	1.4	1.3	1.2	1.1	1.0
cosθ	0.9981	0.9952	0.0680	0.0653	-0.0079

IV. Partial Discharge Statistical Characteristics and Identification of Typical Samples

A. Statistical Characteristics of Three Typical Discharges

Observing the PD pulses extracted from the silicone gel, DBC-silicone gel interface and chip samples, the discharges of the three samples have certain differences in PD pulse repetition rate, pulse amplitude, discharge polarity, and distribution characteristics in the time domain. Due to the randomness of PDs, it is necessary to investigate the statistical PD characteristics of the silicone gel, DBC-silicone gel interface, and chip samples further.

In the following, five cycles of current signals are collected at each time, and at least 10 times are collected to recognize the statistical PD characteristics of typical discharge positions in high voltage IGBT modules.

TABLE III
PARTIAL DISCHARGE PARAMETERS OF SILICONE GEL SAMPLE UNDER DIFFERENT VOLTAGES

Voltage (kV)	18.00	19.00	20.00
PD repetition rate (s^{-1})	200.00	251.00	186.00
Average pulse amplitude (mA)	0.34	0.38	0.84
Positive discharge ratio	45.45 %	48.20 %	53.22 %
Variation stage discharge ratio	96.36 %	91.24 %	88.71 %

TABLE IV
PARTIAL DISCHARGE PARAMETERS OF DBC-SILICONE GEL INTERFACE SAMPLE UNDER DIFFERENT VOLTAGES

Voltage (kV)	19.30	20.30	21.30
PD repetition rate (s^{-1})	191.00	329.00	579.29
Average pulse amplitude (mA)	4.97	4.62	8.82
Positive discharge ratio	51.31 %	54.10 %	58.82 %
Variation stage discharge ratio	19.09 %	34.24 %	78.45 %

TABLE V
PARTIAL DISCHARGE PARAMETERS OF CHIP UNDER DIFFERENT VOLTAGES

Voltage (kV)	4.40	4.46	4.52
PD repetition rate (s^{-1})	718.33	9640.00	69710.00
Average pulse amplitude (mA)	0.33	0.38	0.33
Positive discharge ratio	100.00 %	100.00 %	100.00 %

PD parameters of each sample under different voltages are given in Table III–V, where PD repetition rate is the ratio of discharge quantity to time, and average pulse amplitude is the average absolute value of pulse peak value. The positive discharge ratio is the ratio of positive polarity PD pulse to the total number of pulses. The variation stage discharge ratio represents the proportion of the number of discharges occurring in t_c time as shown in Fig. 5 to the total number of discharges.

The PD amplitude of DBC-silicone gel sample is larger than that of silicone gel and chip samples. The ratio of positive polarity discharge of silicone gel and DBC is close to 50%, while that of a chip is 100%. In addition, the discharge repetition rate of the chip is significantly higher than that of the silicone gel and DBC-silicone gel interface samples.

With the increase of voltage, the PD amplitude of the silicone gel and DBC-silicone gel interface sample increases evidently, but the amplitude of the latter is still larger than that of the former. The variation stage discharge ratio of the silicone gel sample gradually decreases, but still more than 85%, and that of the DBC-silicone gel sample increased from 19% to 78%. The PDs of the chip are still positive at different voltages, and the pulse amplitude is almost unchanged, but the discharge repetition rate increases by two orders of magnitude with the increase of voltage.

To intuitively obtain the PD distribution characteristics of silicone gel, DBC-silicone gel, and chip under positive square wave voltage, the PD pulses with timestamps in the 50 cycles are counted in the same cycle by time-resolved PD (TRPD) pattern [30] as shown in Fig. 12. Because of the similarity of the three voltage waveforms, only one voltage waveform is selected as a reference.

The forward and backward discharges of the silicone gel are concentrated in 0–0.05 ms and 10–10.05 ms, with the amplitude

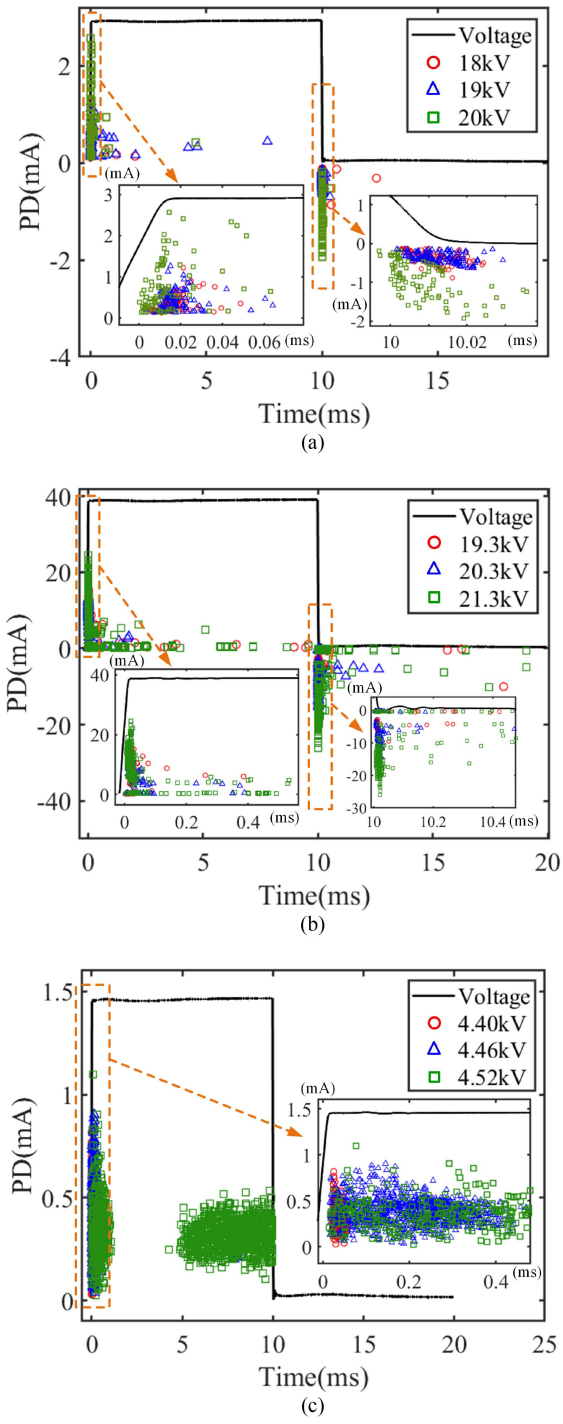

Fig. 12. TRPD pattern of three samples at different voltages. (a) Silicone gel. (b) DBC-Silicone gel interface. (c) Chip.

of 0–3 mA. The discharge pattern forms a "∠" shape at each applied positive square wave voltage both for the forward and backward discharges. Besides, the higher the voltage level is, the earlier the discharge occurs.

PDs of the DBC-silicone gel sample are distributed at the voltage rising edge, falling edge, and the voltage steady-state. The PD amplitude in the variation stage is mainly concentrated in 0–20 mA, higher than that in the voltage steady-state. The

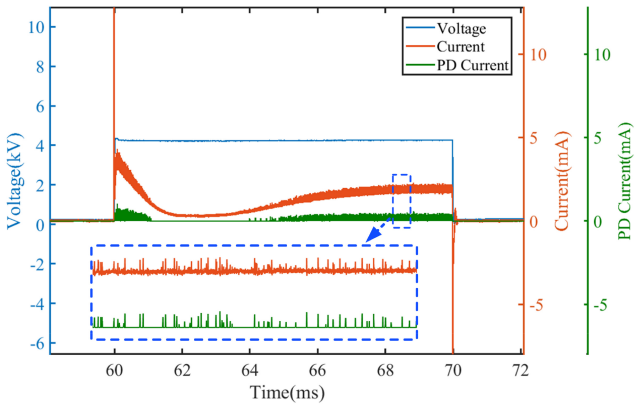

Fig. 13. Chip PD pulses at 4.52kV.

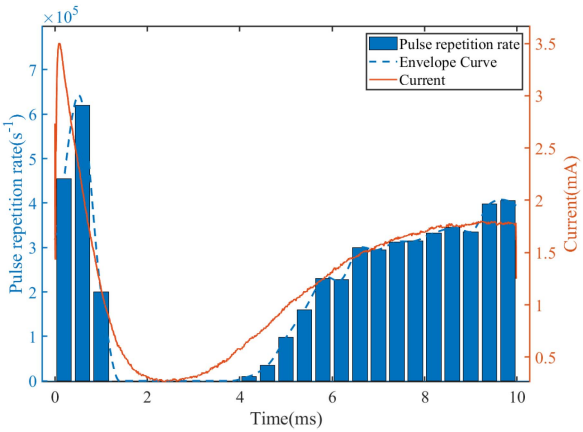

Fig. 14. PD pulse repetition rate and leakage current of the chip.

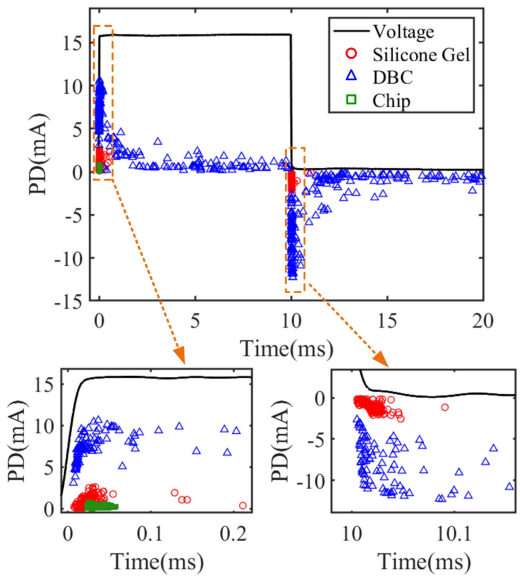

Fig. 15. TRPD pattern of three samples.

TABLE VI
PARTIAL DISCHARGE PARAMETERS OF THREE SAMPLES

Sample	Silicone gel	DBC- silicone gel interface	Chip
PD repetition rate (s^{-1})	237.14	213.68	698.33
Average pulse amplitude (mA)	0.89	4.30	0.33
Positive discharge ratio	56.83%	49.75%	100%
Variation stage discharge ratio	88.19%	28.54%	76.57%

TRPD of DBC-silicone gel is shaped like "L" and "T" for the forward and backward discharges. As the voltage level increases, the pattern is more dispersed.

While for the discharges in the chip, the TRPD pattern of the chip changes greatly under different voltages. At 4.40 kV, the chip discharge only concentrates in 0–0.1 ms, and the amplitude concentrates in 0–1 mA. As the voltage rises to 4.52 kV, discharges spread at 0–1 ms and 5–10 ms. Besides, the voltage, leakage current, and discharge pulses of the chip at 4.52 kV are plotted in Fig. 13. It is found that the leakage current of the chip presents a waveform like "√" during the high voltage steady-state.

By comparing the discharge pulses and current waveform as shown in Fig. 13, it is found that the similarity between the PD pulse repetition rate and leakage current amplitude is 0.9275. As shown in Fig. 14, each blue bar represents the pulse repetition rate within 0.4 ms, the blue dotted line is the envelope curve of PD pulse repetition rate, and the red curve is the current waveform.

B. PD Identification of Typical Samples and its Application Scenarios

To verify the feasibility of PD parameters and TRPD patterns in the PD identification of modules under the positive repetitive square wave voltage, the PD pulses of the silicone gel, DBC-silicone gel interface, and chip samples under their respective RPDIV are extracted. The TRPD patterns of each sample under RPDIV are plotted in Fig. 15.

Besides, the corresponding discharge parameters for the samples are given in Table VI. The positive discharge ratio of the chip is 100%, which is the key parameter to distinguish the chip discharge from the other two kinds of discharges, and the PD repetition rate can also be used as an auxiliary parameter to identify chip discharges. Meanwhile, the average pulse amplitude and variation stage discharge ratio can be used to distinguish the PDs between silicone gel and DBC-silicone gel interface because PD pulses of silicone gel have smaller amplitude and more distribution in the voltage variation stage.

Therefore, the differences in PD characteristics of typical structures of high voltage modules under positive square wave voltage are summarized as follows.

1) The PD pulses of a chip are positive, and its repetition rate increases significantly with the increase of voltage.
2) Both forward and backward current pulses can be generated for silicone gel. The PD current pulses tend to concentrate in the voltage variation state, shaping "∠" in the TRPD distribution.
3) Both forward and backward current pulses can be generated for the DBC-silicone gel interface. The PD pulses

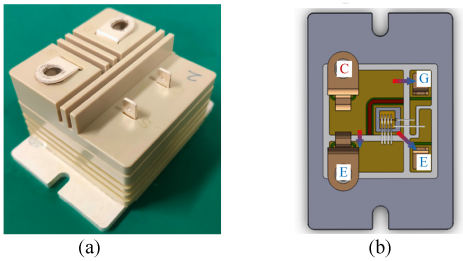

Fig. 16 Wire-bond module sample. (a) External structure. (b) Internal structure.

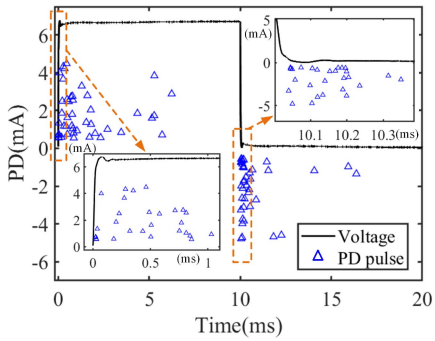

Fig. 17 TRPD pattern of the wire-bond module's discharges.

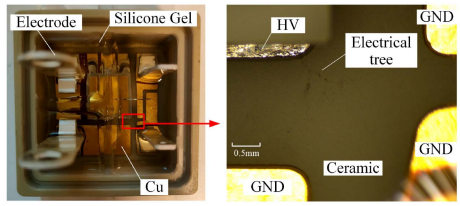

Fig. 18. Electrical tree on the DBC ceramic of wire-bond module sample.

tend to have larger amplitudes in the voltage variation stage and have more dispersion in the time domain than that of silicone gel. The TRPD pattern of DBC-silicone gel is shaped like "L" and "Γ."

The application scenarios of the method proposed in this article are as follows. First, in the module design stage, the reliability of the proposed insulation structure can be tested under the operating voltage, and then the insulation structure with defects can be modified pointedly according to the PD identification results. Second, in the module production stage, the insulation reliability of the modules can be tested, and then the specific defect type can be determined according to the PD identification method without destroying the integrity of the module.

C. Experimental Verification of the PD Identification Method

To verify the effectiveness of the proposed PD identification method in practical application, a wire-bond module without a chip is designed and manufactured.

The external and internal structures of the module are shown in Fig. 16(a) and (b), respectively. The module is well enclosed, and except for without the chip, the structure of the package is designed according to the actual wire-bond module. This module can be used to find the possible weak point of the package in the design stage of a module. In this module, the chip is replaced by a DBC structure that can withstand 40 kV voltage.

In the experiment, positive repetitive square wave voltage is applied on the collector of the module shown in Fig. 16, and the gate and emitter are grounded. It should be emphasized that the module is sealed by the external structure, so it can be considered as a black-box macroscopically for the discharge position. During the experiment, PDs occur in the module at 14.3 kV finally. Through the pulse extraction method, the PD pulses of the module are extracted, and its TRPD pattern is drawn in Fig. 17.

It can be seen that the TRPD pattern shown in Fig. 17 is shaped like "L" and "Γ" and has more dispersion in the time domain. According to the identification method proposed, it is consistent with the discharge characteristics of the DBC-silicone gel interface.

To verify the accuracy of the identification method, the external tube of the module is disassembled. The electric tree near the DBC interface can be clearly identified as shown in Fig. 18. According to the position of the electric tree, the discharges belong to the DBC-silicone gel surface discharges, which confirms the accuracy of the above judgment. Therefore, through the identification method, it can be judged that the surface discharges of DBC-silicone gel occurred inside the module without destroying its integrity.

In summary, the PD pulse extraction and PD identification methods proposed in this article can provide certain guidelines for the design and manufacture of the high voltage modules.

It should be pointed that with the development of high voltage modules, more encapsulation materials, such as epoxy resin and silicone elastomers are used for module packaging and the discharge characteristics will be required further investigation.

V. Discussion

The basic cause of PD in insulating materials is that the partial field strength exceeds the critical initial field strength due to the defects or in the non-uniform electric field. The distribution of the electric field depends not only on the applied voltage but also on the space charge.

Assuming that the electric field intensity caused only by the applied voltage at a certain point in the insulation material is $\boldsymbol{E}_u$, and the electric field intensity caused only by the space charge is $\boldsymbol{E}_c$. Thus, the actual field intensity $\boldsymbol{E}_r$ at a certain point can be expressed as

$$\boldsymbol{E}_r = \boldsymbol{E}_u + \boldsymbol{E}_c. \tag{9}$$

In the following, the discharge mechanisms of silicone gel, DBC-silicone gel interface, and chip under positive square wave voltage will be qualitatively explained.

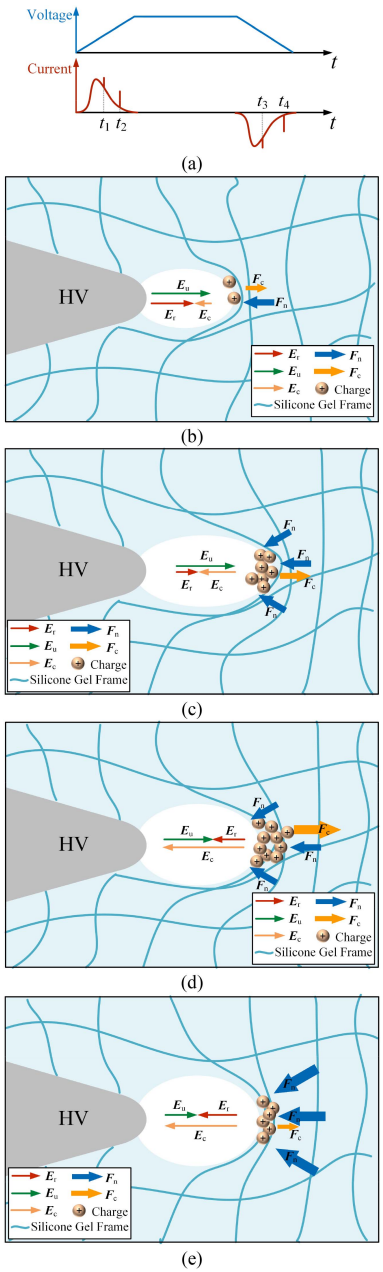

Fig. 19. Discharge mechanism of silicone gel. (a) Time domain diagram of PD pulse, (b) t_1, (c) $t_1{}^+$, (d) t_3, and (e) t_4.

A. Silicone gel

For the discharge of the silicone gel in this article, the discharge usually occurs at the tiny bubbles in silicone gel around the needle with a high electric field [11]. The schematic figure of the discharge in silicone gel is shown in Fig. 19.

The applied voltage increases gradually at the rising edge, and PD occurs when the field intensity $\boldsymbol{E}_r$ inside the bubble is greater than the critical field intensity of discharge $\boldsymbol{E}_0$ at t_1, as shown in Fig. 19(b). Then, a large number of electrons is rapidly driven to the anode side at t_1, causing the positive current pulses. Then, accompanied with the positive space charges at the cathode side, the reverse electric field can be generated right after t_1, which will weaken the field intensity $\boldsymbol{E}_r$ inside the bubble, as shown in Fig. 19(c). As a result, the continuous discharge is inhibited. Besides, due to the bubble expansion caused by the discharge at t_1, the cross-linked polymer network of the silicone gel is squeezed and deformed as shown in Fig. 19(c), causing the bubble walls to be subjected to elastic forces $\boldsymbol{F}_n$ from the polymer network, tending to reshape the bubble. Meanwhile, the accumulated positive space charges on the cathode side of the bubble wall are subjected to the electric field force $\boldsymbol{F}_c$ in the same direction as the electric field, keeping the expansion of the bubble wall. Then, the applied electric field further increases with time, and the electric field $\boldsymbol{E}_r$ increases to $\boldsymbol{E}_0$ again at t_2. However, due to the expansion of the distance between both sides of the bubble, the electric potential difference on them at t_2 is larger than that at t_1, resulting in more intense discharge at t_2, which is reflected in the amplitude of PD current pulses. Thus, in terms of statistical properties, it has a trend of increasing discharge amplitude with time, leading to the "$\angle$" shaped TRPD pattern of the silicone gel.

A few discharges occur in the high voltage steady-state because the migration rate of the carriers inside the silicone gel is about 10^{-12} $m^2 \bullet V^{-1} \bullet s^{-1}$, which is greater than that of the solid insulation material [25], thus the accumulated positive charges migrate to the cathode continuously, enhancing $\boldsymbol{E}_r$ and eventually leading to PD.

At the falling edge of the voltage, $\boldsymbol{E}_u$ decreases rapidly, then a reverse electric field is formed in the bubble by the accumulated positive space charges, as shown in Fig. 19(d) Then, backward discharge occurs at t_3, when $\boldsymbol{E}_r$ is greater than the critical field intensity $\boldsymbol{E}_0$. After that, the reverse $\boldsymbol{E}_r$ decreases due to the reduction of charges, restraining the continuous discharge. As the voltage continues to decrease, discharge occurs at t_4 with the increase of field intensity $\boldsymbol{E}_r$ and the decrease of residual charges similar to the forward discharge. However, the electric field force $\boldsymbol{F}_c$ is weakened as the voltage drops and the charge decreases, so the elastic forces $\boldsymbol{F}_n$ from the polymer network gradually come to dominate. Thus, the expansion of the bubble cannot be maintained, so the rising tendency of the amplitude of backward discharges with time is less than that of forward discharges as shown in Figs. 12(a) and 15.

Different from the high voltage steady-state, there is no directional charge migration in the low voltage steady-state, so almost no discharge occurs. As the voltage level increases, the field intensity $\boldsymbol{E}_r$ in the bubbles reaches $\boldsymbol{E}_0$ faster, so the discharge occurs earlier, which is reflected in the left shift of the green marker in Fig. 12(a). Besides, the increase of field strength will lead to the acceleration of charge migration in the high voltage steady-state. What falls is the increase of the number of discharges in the high voltage steady-state, resulting in the decrease in the variation stage discharge ratio in Table III.

B. DBC-silicone gel interface

The joint action of residual charges and electric field changes for discharges in the DBC-silicone gel interface is similar to that in silicone gel, but one of the significant differences is that for the dynamic streamer discharge along the surface, time-lag plays a critical role under positive square wave voltage [18].

For the forward discharge, when $\boldsymbol{E}_r$ near the anode exceeds $\boldsymbol{E}_0$, it still needs to experience the free electron supply time and the avalanche build-up time before the discharge occurs. As a result, when PD occurs at t_5, $\boldsymbol{E}_r$ is far higher than $\boldsymbol{E}_0$, so discharges in DBC-silicone gel interface are more intense and the pulse amplitude is relatively higher than those in silicone gel. Meanwhile, discharges in DBC-silicone gel interface have a larger variation stage discharge ratio than that of silicone gel due to this time-lag. Besides, the randomness of the time-lag explains the distinct dispersion of the DBC discharge pattern near the rising edge. The mechanism of backward discharge at t_7 also has similar features. However, in the high voltage steady state, the electric field changes caused by charge migration in the silicone gel are much less rapid than those caused by voltage rising state in the variation state, so time-lag has much less effect on the discharges in the high voltage steady-state. Thus, the discharge amplitude at t_6 is much smaller than that at t_5, explaining the "L" shaped TRPD pattern of the DBC-silicone gel interface.

Besides, the other difference is reflected in the force on the bubbles. Due to the more positive charges than in silicone gel gathered at the cathode side of the bubble as shown in Fig. 20(b), the bubble is stretched longer than in silicone gel by the electric field force $\boldsymbol{F}_c$ as shown in Fig. 20(c). In the low voltage steady-state, the applied electric field disappears, so the bubble wall is only subjected to the elastic force of the silicone gel crosslinked polymer network, which will shrink the bubble. Meanwhile, there is no directional transfer of charges during this period, so the charge near the bubble wall is concentrated with the bubble shrinking, which increases the field intensity in the bubble and leads to the occurrence of the backward discharge at t_8. However, due to the discharge at t_7, there are less residual positive charges to discharge, so the amplitude of backward discharge in the low voltage steady-state is small, resulting in the " Γ " shaped TRPD pattern.

Furthermore, two reasons can attribute to the significant increase of DBC variation stage discharge ratio with voltage level. First, with the increase of voltage level, the discharge time-lag becomes shorter, which leads to part of the discharge occurring in the voltage variation state. Second, the structure of double-sided copper makes the electric field distribution near the electrode tip more dispersed, so the voltage rise will cause more discharges in different directions, which leads to the increase in the number of discharges during the voltage variation and the fan-shaped electrical tree on DBC shown in Fig. 21. Thus, the discharge repetition rate of DBC-silicone gel interface increases significantly with the increase of voltage.

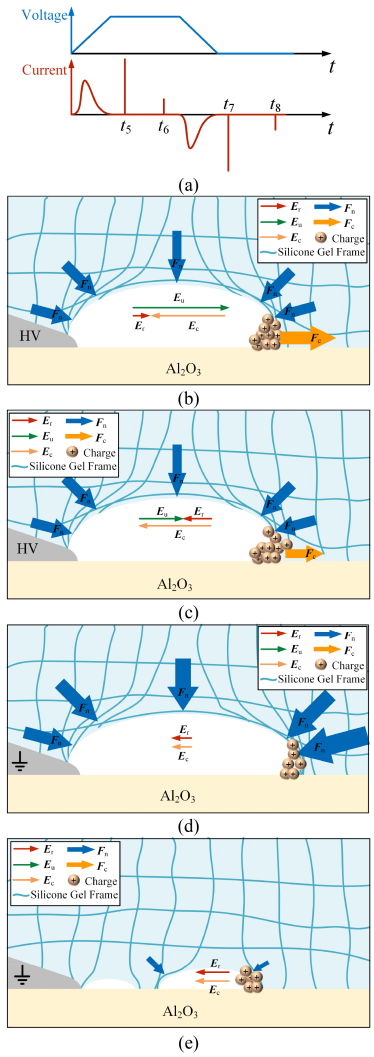

Fig. 20. Discharge mechanism of DBC-silicone gel interface. (a) Time domain diagram of PD pulse, (b) t_5^+, (c) t_7, (d) t_7^+, and (e) t_8

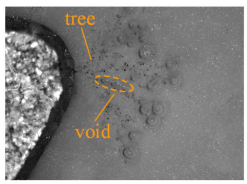

Fig. 21. Electrical trees and voids on the DBC- silicone gel interface.

C. Chip

For semiconductor chips, PDs tend to occur at the terminal region, where have the maximum electric field strength [31]. So, as shown in Fig. 12(c), the discharges of chip only distribute in the high voltage steady-state, when there will be enough field intensity.

When the electric potential difference between the two sides of the space charge region (SCR) rises to a certain threshold, the voltage between the two sides of the internal defect gradually increases and PD occurs. Due to the dense wafer, the internal defects are small. After the discharge occurs, electrons rapidly migrate from the cathode side of the air gap to the anode side, forming a reverse electric field that, can hinder the continuous development of the discharge in a short time. Thus, the discharge pulse amplitude is small.

Due to the properties of semiconductors, the charge will immediately migrate to the two sides of SCR under the action of the electric field and then the next discharge will occur. Meanwhile, as carriers are depleted in the SCR, thermally generated

electron-hole pairs will migrate to the two sides of SCR, resulting in the leakage current as shown in Fig. 13. Thus, the discharge repetition rate of the chip is strongly correlated with the leakage current amplitude because of the similarity of the two processes.

VI. Conclusion

A PD experimental platform for the insulation structure of high voltage IGBT module under square wave voltage is established and PD characteristics of typical discharge locations are obtained. The specific conclusions are obtained.

1) A PD experiment platform under positive square wave voltage is established for silicone gel, DBC-silicone gel interface and chip, which are the typical discharge position in high voltage IGBT module. The current signals of PD of three samples are measured by the HFCT method. According to the obtained current signals, a method of PD pulse current extraction without other auxiliary detection means is proposed, and the accurate extractions of PD pulses from three samples under the interference of displacement current are realized.
2) The key parameters and phase distributions of three typical PDs are analyzed statistically. The discharge current pulses of chip are positive and only appear in the high voltage steady-state. The amplitude range is 0–1 mA, and the discharge repetition rate is strongly correlated with the leakage current. Forward positive discharge current pulses and backward negative current pulse can be generated both for the silicone gel and DBC-silicone gel interface. The discharge only appears in the voltage variation stage and the amplitude is concentrated in 0–5 mA. But the discharge amplitude of the DBC-silicone gel interface is mainly concentrated in 5–10 mA at the voltage variation stage and 0–5 mA at the voltage steady stage.
3) Based on the differences in the PD characteristics from the three typical structures, the discharge types can be identified. The discharge of chip can be distinguished from that of package insulation by pulse polarity, discharge repetition rate, TRPD distribution, and even leakage current waveform. PDs in silicone gel mainly concentrate in the voltage variation state and shaping "$\angle$" in the TRPD, but PDs in DBC-silicone gel interface have more dispersion in voltage steady-state than that of silicone gel. Experiments are conducted to demonstrate the effectiveness and practicality of the proposed method. By analyzing the combined effect of applied voltage and space charge and considering the effect of bubble volume change in silicone gel on discharge, the mechanism of discharge and related characteristics are explained qualitatively.

References

[1] H. Wang, J. Przybilla, H. Zhang, and J. Schiele, "A new press pack IGBT for high reliable applications with short circuit failure mode," *CPSS Trans. Power Electron. Appl.,* vol. 6, no. 2, pp. 107–114, Jun. 2021.

[2] Y. Luo, F. Xiao, B. Liu, and Y. Huang, "A physics-based transient electrothermal model of high-voltage press-pack igbts under HVDC interruption," *IEEE Trans. Power Electron.,* vol. 35, no. 6, pp. 5660–5669, Jun. 2020.

[3] E. Van Brunt et al., "27 kV, 20 A 4H-SiC n-IGBTs," *Mater. Sci. Forum*, vol. 821, pp. 847–850, 2015.

[4] R. Simpson, A. Plumpton, M. Varley, C. Tonner, P. Taylor, and X. Dai, "Press-pack IGBTs for HVDC and facts," *CSEE J. Power Energy Syst.,* vol. 3, no. 3, pp. 302–310, Sep. 2017.

[5] I. Semenov, I. F. Gunheim, K. Niayesh, H. K. H. Meyer, and L. Lundgaard, "Investigation of partial discharges in AlN substrates under fast transient voltages," *IEEE Trans. Dielect. Elect. Insul.,* vol. 29, no. 2, pp. 745–752, Apr. 2022.

[6] M. Ghassemi, "PD measurements, failure analysis, and control in high-power IGBT modules," *High Voltage,* vol. 3, no. 3, pp. 170–178, 2018.

[7] J. Fabian, S. Hartmann, and A. Hamidi, "Analysis of insulation failure modes in high power IGBT modules," in *Proc. IEEE 40th IAS Annu. Meeting Conf. Rec. Ind. Appl. Conf.*, 2005, vol. 2, pp. 799–805.

[8] G. Mitic and G. Lefranc, "Localization of electrical-insulation and partial-discharge failures of IGBT modules," *IEEE Trans. Ind. Appl.,* vol. 38, no. 1, pp. 175–180, Jan./Feb. 2002.

[9] M. Morshed et al., "High temperature polyimide polymer material for high voltage IGBT power module switching applications," in *Proc. IEEE 20th Eur. Conf. Power Electron. Appl.*, 2018, pp. P.1–P.7.

[10] M. Sato, A. Kumada, K. Hidaka, K. Yamashiro, Y. Hayase, and T. Takano, "Surface discharges in silicone gel on AlN substrate," *IEEE Trans. Dielect. Elect. Insul.,* vol. 23, no. 1, pp. 494–500, Feb. 2016.

[11] H. You, Z. Wei, B. Hu, Z. Zhao, R. Na, and J. Wang, "Partial discharge behaviors in power modules under square pulses with ultrafast dv/dt," *IEEE Trans. Power Electron.,* vol. 36, no. 3, pp. 2611–2620, Mar. 2020.

[12] M. T. Do, J. I. Auge, and O. Lesaint, "Partial discharges in silicone gel in the temperature range 20-150°C," in *Proc. IEEE Conf. Elect. Insul. Dielect. Phenomena*, 2006, pp. 590–593.

[13] M. T. Do, O. Lesaint, and J. I. Auge, "Partial discharges and streamers in silicone gel used to encapsulate power electronic components," in *Proc. IEEE Annu. Rep. Conf. Elect. Insul. Dielect. Phenomena*, 2007, pp. 155–158.

[14] W. Yabuuchi et al., "Electric field strength and tree propagation speed for electrical treeing in silicone gel," in *Proc. IEEE Int. Symp. Elect. Insul. Mater.*, 2020, pp. 474–477.

[15] Y. Wang et al., "Space-charge accumulation and its impact on high-voltage power module partial discharge under DC and PWM waves: Testing and modeling," *IEEE Trans. Power Electron.,* vol. 36, no. 10, pp. 11097–11108, Oct. 2021.

[16] M. T. Do, J. L. Auge, and O. Lesaint, "Optical measurement of partial discharges in silicone GEL under repetitive pulse voltage," in *Proc. IEEE Int. Symp. Elect. Insul. Mater.*, 2005, vol. 2. pp. 360–363.

[17] P. Mancinelli, A. Cavallini, N. Chalashkanov, S. J. Dodd, and L. A. Dissado, "Electrical treeing in silicone gel under square voltage: Frequency, rise time and crosslinking influence," in *Proc. IEEE Conf. Elect. Insul. Dielect. Phenomena*, 2016, pp. 979–982.

[18] P. Fu, Z. Zhao, X. Li, X. Cui, and Z. Yang, "The role of time-lag in the surface discharge inception under positive repetitive pulse voltage," *Phys. Plasma,* vol. 25, no. 9, 2018, Art. no. 093518.

[19] S. Nakamura et al., "Electrical treeing in silicone gel under repetitive voltage impulses," *IEEE Trans. Dielect. Elect. Insul.,* vol. 26, no. 6, pp. 1919–1925, Dec. 2019.

[20] Y. Wang, Z. Yuan, H. Peng, Y. Ding, Y. Yin, and L. Fang, "Partial discharge testing platform for high voltage power module packaging under square wave excitation," in *Proc. IEEE Appl. Power Electron. Conf. Expo.*, 2021, pp. 1491–1495.

[21] Y. Lin et al., "Temperature- and degradation- dependent maximum electric field stress in wire-bonding power modules under PWM waves," *IEEE J. Emerg. Sel. Topics Power Electron*, vol. 10, no. 6, pp. 7653–7664, Dec. 2022, doi: 10.1109/JESTPE.2022.3195177.

[22] T. Lebey, D. Malec, S. Dinculescu, V. Costan, F. Breit, and E. Dutarde, "Partial discharges phenomenon in high voltage power modules," *IEEE Trans. Dielect. Elect. Insul.,* vol. 13, no. 4, pp. 810–819, Aug. 2006.

[23] P. Fu et al., "Partial discharge measurement and analysis in PPIs," *IET Power Electron,* vol. 12, no. 1, pp. 138–146, 2019.

[24] *Electrical Insulating Materials and Systems – Electrical Measurement of Partial Discharges (PD) Under Short Rise Time and Repetitive Voltage Impulses*, IEC TS 61934, 2011.

[25] J. Xu, X. Li, X. Cui, Z. Zhao, S. Mo, and B. Ji, "Trap characteristics and their temperature-dependence of silicone gel for encapsulation in IGBT power modules," *CSEE J. Power Energy Syst.,* vol. 7, no. 3, pp. 614–621, May. 2021.

[26] *High-Voltage Test Techniques–Partial Discharge Measurements*, IEC 60270-2015, 2015.
[27] R. Sargazi, A. Akbari, P. Werle, and H. Borsi, "A novel wideband partial discharge measuring circuit under fast repetitive impulses of static converters," *Measurement,* vol. 178, 2021, Art. no. 109353.
[28] C. Zhang, Y. Xu, M. Dong, R. Burgos, M. Ren, and D. Boroyevich, "Design and assessment of external insulation for critical components in a medium voltage SiC-based converter via optical method," *IEEE Trans. Power Electron.*, vol. 35, no. 12, pp. 12887–12897, Dec. 2020.
[29] F. Guastavino, A. Dardano, and E. Torello, "Measuring partial discharges under pulsed voltage conditions," *IEEE Trans. Dielect. Elect. Insul.,* vol. 15, no. 6, pp. 1640–1648, Dec. 2008.
[30] H. Xu, G. Wu, G. Zhu, Y. Luo, K. Cao, and Y. Zhang, "Analysis of partial discharge characteristics of frequency conversion motor strand under high frequency square wave pulse," *Adv. Technol. Elect. Energy,* vol. 31, no. 04, pp. 48–108, 2012.
[31] Z. Liu et al., "A novel chip surface shielding structure for promoting insulation capability of high voltage semiconductor chip," *IEEE Trans. Electron. Devices,* vol. 69, no. 1, pp. 439–443, Jan. 2022.

Xiangchen Liu was born in Jiangsu, China in 1997. He received the B. Sc. degree in electrical engineering from China University of Mining and Technology, Xuzhou, China, in 2020. He is currently working toward the M.Sc. degree in electrical engineering with the North China Electric Power University, Beijing, China.

His current research interest includes electrical insulation for high voltage devices.

Xuebao Li was born in Tianjin, China, in 1988. He received the B.Sc. and Ph.D. degrees in electrical engineering from the North China Electric Power University, Beijing, China, in 2011 and 2016, respectively.

He is currently an Associate Professor with the School of Electrical and Electronic Engineering, North China Electric Power University. His research interests include the electromagnetic environment and electromagnetic compatibility in power systems, and insulation problems in high-voltage apparatus.

Chao Li was born in Hohhot, China, in 1996.He received the B.Sc. degree in smart grid information engineering in 2019 from North China Electrical Power University, Beijing, China, where he is currently working toward the M.Sc. degree in electrical engineering.

His research interests include insulation problems of power devices.

Jinjin Cheng was born in Henan, China, in 1996. She received the B.Sc. and M.Sc. degrees in electrical engineering from the North China Electrical Power University, Beijing, China, in 2018 and in 2022.

She is currently an Engineer with State Grid Henan Extra High Voltage Company, Xinyang, China. Her research interests include insulation problems of power devices.

Zhaocheng Liu was born in Hebei, China, in 1996. He received the B. Sc. degree in electrical engineering in 2019 from North China Electrical Power University, Baoding, China, where he is currently working toward the Ph.D. degree in electrical engineering.

His research interests include insulation problems of power devices.

Zhibin Zhao was born in Hebei, China, in 1977. He received the Ph.D. degree in electrical engineering from the North China Electric Power University, Baoding, China, in 2005.

He is currently a Professor with the State Key Laboratory of Alternate Electrical Power System, Renewable Energy Sources, North China Electric Power University. His main research interests include computational electromagnetics and electromagnetic compatibility in power electronic.

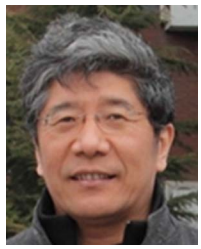

Xiang Cui (Senior Member, IEEE) was born in Baoding, Hebei Province, China, in 1960. He received the B.Sc. and M.Sc. degrees in electrical engineering from North China Electric Power University, Baoding, China, in 1982 and 1984, respectively, and the Ph.D. degree in accelerator physics from the China Institute of Atomic Energy, Beijing, China, in 1988.

He is currently a Professor and the Vice Director of the State Key Laboratory of Alternate Electrical Power System with Renewable Energy Sources, North China Electric Power University. His research interests include computational electromagnetics, electromagnetic environment and electromagnetic compatibility in power systems, insulation and magnetic problems in high-voltage apparatus.

Dr. Cui is a Standing Council Member of the China Electrotechnical Society and a Fellow of *IET*. He is also an Associate Editor for IEEE TRANSACTIONS ON ELECTROMAGNETIC COMPATIBILITY.

Xiaoguang Wei received the Bachelor of Engineering and Master of Engineering degrees from the North China Electric Power University, Beijing, China, in 1999 and 2003, respectively, and the Ph.D. degree in engineering from China Electric Power Research Institute, Beijing, China, in 2007.

He is currently with State Grid Smart Research Institute, Power Semiconductor Technology Research Department, Beijing, China. His research interests include HVdc transmission, dc power grid, and power semiconductor devices.

Xinling Tang received the B.Sc. degree from North China Electric Power University, Beijing, China, in 2011, and the M. S. degree from Shanghai Jiao Tong University, Shanghai, China, in 2014, and the Ph.D. degree from North China Electric Power University, Beijing, in 2017, all in electrical engineering.

His research interests include power semiconductor devices and electromagnetic modeling of high voltage high power semiconductor devices for HVdc application.